Published in final edited form as:
Biochemistry. 2006 July 4; 45(26): 7949–7958. doi:10.1021/bi052182l.

Electrostatic Environment of Hemes in Proteins: pK_as of Hydroxyl Ligands†

Yifan Song, **Junjun Mao**, and **M. R. Gunner***
Physics Department J-419, City College of New York, 138th Street and Convent Avenue, New York, New York 10031

Abstract

The pK_as of ferric aquo–heme and aquo–heme electrochemical midpoints (E_ms) at pH 7 in sperm whale myoglobin, *Aplysia* myoblogin, hemoglobin I, heme oxygenase 1, horseradish peroxidase and cytochrome *c* oxidase were calculated with Multi-Conformation Continuum Electrostatics (MCCE). The pK_as span 3.3 pH units from 7.6 in heme oxygenase 1 to 10.9 in peroxidase, and the E_ms range from −250 mv in peroxidase to 125 mV in *Aplysia* myoglobin. Proteins with higher in situ ferric aquo–heme pK_as tend to have lower E_ms. Both changes arise from the protein stabilizing a positively charged heme. However, compared with values in solution, the protein shifts the aquo–heme E_ms more than the pK_as. Thus, the protein has a larger effective dielectric constant for the protonation reaction, showing that electron and proton transfers are coupled to different conformational changes that are captured in the MCCE analysis. The calculations reveal a breakdown in the classical continuum electrostatic analysis of pairwise interactions. Comparisons with DFT calculations show that Coulomb's law overestimates the large unfavorable interactions between the ferric water–heme and positively charged groups facing the heme plane by as much as 60%. If interactions with Cu_B in cytochrome *c* oxidase and Arg 38 in horseradish peroxidase are not corrected, the pK_a calculations are in error by as much as 6 pH units. With DFT corrected interactions calculated pK_as and E_ms differ from measured values by less than 1 pH unit or 35 mV, respectively. The in situ aquo–heme pK_a is important for the function of cytochrome *c* oxidase since it helps to control the stoichiometry of proton uptake coupled to electron transfer

Heme cofactors are found in many proteins. Cytochromes having two axial ligands contributed by the protein are six-coordinate and function as redox intermediates in electron transfer chains. However, five-coordinate hemes with one His ligand and one open position are the most common heme motif (1). The open site can bind different molecules for transport or catalysis. Hemoglobins and myoglobins are O_2 transporters (2). Heme oxygenase is an essential protein in heme metabolism, using three O_2s and seven electrons to degrade heme to biliverdin (3). Peroxidases reduce toxic hydrogen peroxide to water and then carry out one electron oxidization of a wide range of substrates (4,5). Cytochrome *c* oxidase is the terminal electron acceptor in the respiratory chain (6–9). Here Heme *a*3 forms a binuclear center with a copper complex (Cu_B) that reduces O_2 to water. The protein uses the released chemical energy to pump protons across the membrane. Other five-coordinate heme proteins carry out NO storage and transport (10), steroid synthesis (11,12), and O_2, CO, and NO sensing (13,14).

†This work is supported by NIH Grant RO1-GM64540.

*To whom correspondence should be addressed. Telephone: 212-650-5557. Fax: 212-650-6940. E-mail: gunner@sci.ccny.cuny.edu.

SUPPORTING INFORMATION AVAILABLE

Interactions between heme *a*3 and CuB in different aquo protonation and cofactor redox states calculated in a vacuum by Coulomb's law and by DFT using Gaussian 98 and in cytochrome *c* oxidase embedded in a low dielectric slab surrounded by water using DelPhi. This material is available free of charge via the Internet at http://pubs.acs.org.

Hemes can carry out many biological functions because the protein, especially the active site residues, modulates the ligand binding specificity and resultant chemistry. The diversity of in situ heme functions highlights important interactions of proteins with their cofactors and substrates. Extensive studies have explored how ligand geometry (15–17) and the protein scaffolding (18) affect in situ heme properties (1). The range of redox free energy and pK_as of protein-bound hemes and their ligands show the importance of electrostatic interactions (19, 20). For example, six-coordinate bis-His–hemes have E_ms ranging from −410 to +360 mV with the redox differences being predominately due to the intraprotein electrostatic environment (1,20–22). In these proteins the loss of solvation energy (15,23,24), interactions with the protein backbone and with other residues (15,20–22,25), and local conformation changes on ionization changes (20,26) determine the thermodynamic equilibrium measured by pK_as and E_ms.

Theoretical studies have analyzed hemes in different systems using a number of techniques. The large span of E_ms in cytochromes has been subject to analysis by Protein Dipole Langevin Dipole (PDLD) (27,28), continuum electrostatics (CE)[1] (20,21,29,30), and other techniques (31–37). E_ms of the two hemes in quinol:fumarate reductase have been determined within 30 mV of experimental values using MCCE, allowing the low- and high-potential heme to be assigned to the distal and proximal positions in the structure (38). The heme propionic acid pK_as and their influence on the pH dependence of cytochrome E_ms have been considered by CE analysis (20,38–40). The pK_as and E_ms of aquo–heme *a*3 and CuB in cytochrome *c* oxidase have been analyzed by CE (41–43) and density functional theory (DFT) (44). DFT and QM/MM calculations have been used to explain the unusual low-spin state of ferric aquo–heme (45–47) and to study the hydroxylation mechanism (48–51) of cytochrome P450.

In the work presented here, pK_as and E_ms of aquo–heme in myoglobins from sperm whale and *Aplysia*, hemoglobin I, heme oxygenase 1, and horseradish peroxidase are calculated with Multi-Conformation Continuum Electrostatics (MCCE) (20,38). The calculated pK_a is compared with the pH of the acid–alkaline transition, which is attributed to the deprotonation of a water molecule as the sixth heme ligand (52). Calculations are also carried out on cytochrome *c* oxidase. Here the pK_a is compared with the pH dependence of the proton release on oxidation of heme *a*3 (53). Several of these proteins have positively charged groups in the active site. The interaction of the heme with these charges is compared in CE and DFT methods, showing that CE overestimates the interaction. With the appropriate corrections, MCCE calculations reproduce the experimental pK_as and E_ms, showing how the protein structures yield the observed in situ reaction energetics. The differences in the shifts of aquo–heme pK_as and E_ms in different binding sites show that electron and proton transfers can be coupled to different active site conformational changes. The aquo–heme E_m is not a factor in the function of myoglobin or hemoglobin, nor are the pK_as important for the reaction mechanism of most of the proteins studied here. However, the aquo–heme pK_a in cytochrome *c* oxidase appears to determine whether heme *a*3 binds a proton during the reduction of the binuclear center (43). Thus, this pK_a helps to control the electroneutrality of the oxidase reduction. The comparison of calculated and measured pK_as and E_ms in the smaller and simpler proteins provides a benchmark for the analysis of the more puzzling oxidase system.

[1]Abbreviations: p$K_{a,sol}$, group pK_a in aqueous solution; $E_{m,sol}$, electrochemical midpoint potential (E_m) of a model for the redox cofactor in aqueous solution; CE, continuum electrostatics; MCCE, Multi-Conformation Continuum Electrostatics; DFT, density functional theory. 1 Δp*K* unit = 1.36 kcal/mol = 58 meV. The propionic acids are designated A and D as found in the PDB structure file. The IUPAC nomenclature calls them respectively propionate D and C.

METHODS

Structures of sperm whale myoglobin (1A6G, 1A6K, 1A6M, 1A6N, 1HJT, 1JP6, and 1JP9), *Aplysia* myoglobin (1MBA and 5MBA), monomeric clam hemoglobin I (1B0B, 1EBT, 1FLP, and 1MOH), rat heme oxygenase 1 (1DVE, 1IVE, 1IX4, 1ULX, and 1VGI), horseradish peroxidase (1ATJ, 1H55, 1H57, 1H58, 1H5A, 1H5C, 1H5D, 1H5E, 6ATJ, and 7ATJ), and *Rhodobacter sphaeroides* cytochrome *c* oxidase (1M56) were obtained from the Protein Data Bank (54). All crystal waters are deleted and protein cavities filled with continuum water. Multi-Conformation Continuum Electrostatics (MCCE) samples both residue ionization state and rotamer position as a function of pH and E_h (55–57). The cytochrome *c* oxidase calculations use the model generated for analysis of proton uptake coupled to anaerobic reduction in MCCE2.0 (43). In this larger protein a rotation angle of 120° is used to make side chain rotamers, reducing the number of conformers. All other calculations use MCCE 2.2, which adds local optimization of side chain positions, pruning to delete energetically indistinguishable conformers and corrections of the CE energy terms for the errors in the dielectric boundary due to extra surface conformations (see www.sci.ccny.cuny.edu/~mcce). Preselected side chain rotamers are generated in 60° increments around each rotatable bond for all amino acids. In each protein, a water or hydroxyl is added to the open heme coordinate position. The aquo–oxygen is placed on the heme iron with square bipyramidal geometry and a 1.95 Å Fe–O bond length. Hydrogens are added in a tetrahedral geometry with a 0.96 Å H–O bond length. Then additional hydroxyl and water conformations are generated in 30° increments around the Fe–O bond, creating 12 conformers for both water and hydroxyl.

Look-up tables are calculated for electrostatic and non-electrostatic conformer self and conformer–conformer pairwise interactions. The electrostatic pairwise interactions and reaction field energies are determined with a finite-difference technique to solve the Poisson–Boltzmann equation using the program DelPhi (58–60). Focusing (61) is used to ensure a final grid spacing of >2 grids/Å. The protein residues are given PARSE charges and radii (62). The protein has a dielectric constant, ε, of 4 while the surrounding water has an ε of 80 with a salt concentration of 150 mM. Cytochrome *c* oxidase is surrounded by a 32 Å slab with $\varepsilon = 4$ placed with IPECE to bury the fewest ionizable residues to simulate the membrane (63). The Lennard-Jones interactions are calculated with AMBER parameters (64), rescaled by 0.25 (65). A metal-centered charge set is used for hemes with a +2 or +3 charge on the ferrous and ferric Fe and −0.5 on each N atom of the porphyrin as used previously in cytochrome benchmark calculations (20,21). The water–heme ligand uses TIP3 charges, and the hydroxyl charge, calculated with B3LYP (66) in Gaussian98 (67), has +0.2 on H and −1.2 on O. For the *a*-type heme in cytochrome *c* oxidase, a +0.3 charge is placed on the formyl group C and −0.3 on O.

MCCE calculates the shift in pK_a or E_m when a group is moved from aqueous solution to the protein. The solution pK_a (p$K_{a,sol}$) and E_m ($E_{m,sol}$) are obtained from measurements in water. p$K_{a,sol}$ for amino acids are taken from studies of peptides (68,69). The heme propionic acids are treated as described previously with a p$K_{a,sol}$ of 4.9 (20). The five-coordinate hemes are assumed to bind a water or hydroxide as the sixth ligand. Heme and its His and water or hydroxide ligands are treated as a complex. A p$K_{a,sol}$ of 9.6 for the hydroxyl in the ferric (70, 71) and 10.9 in the ferrous (71) His–aquo–heme has been measured in microperoxidase 8 (MP8) which has a heme c. The water p$K_{a,sols}$ are assumed to be the same for hemes a and c. The $E_{m,sol}$ for the His–water heme is −120 mV, and −200 mV (72) for the His–hydroxyl heme. The value of −120 mV is slightly higher than the measured value of −140 mV (72,73), giving an 80 mV shift from His–hydroxyl, consistent with the 1.3 pK_a shift between the pK_as of ferric and ferrous aquo–heme (70,71). With the same ligands, the E_m of heme a is 100 (1) to 160 (74,75) mV more positive than that of heme c. An $E_{m,sol}$ of − 20 mV for His–water heme a3 and −100 mV for His–hydroxyl heme a3 is used here. No explicit pairwise interactions of water or hydroxide ligands with the His ligand or heme to which they are bound are considered since

these interactions are included in $E_{m,sol}$ and $pK_{a,sol}$. The reaction field energies in both solution and the protein were calculated for the aquo–heme complexes. A systematic shift of −0.74 Δp*K* unit (−1 kcal/mol) is added to the reference reaction field energy of ferric hydroxyl–heme in the solution ($\Delta G_{RX\text{-}N,sol}$) and 0.5 Δp*K* unit (0.67 kcal/mol) to that of ferrous water–heme. This raises all ferric heme pK_as by 0.74 pH unit and raises the aquo–heme E_ms by 30 mV. Systematic shifts are also applied to the ionized form of ionizable amino acids on the basis of pK_a benchmark studies (43,56,65).

Possible microstates with different ligand and side chain position and protonation states are subjected to Monte Carlo sampling. A microstate is made up of one conformer for each residue, cofactor, and water. The energy of microstate *n* (ΔG^n) is the sum of the electrostatic and nonelectrostatic energies (20):

$$\Delta G^n = \sum_{i=1}^{M} \delta_i \{[\,2.3 m_i k_b T(\mathrm{pH} - pK_{sol,i}) + n_i F(E_h - E_{m,sol,i})] + (\Delta\Delta G_{rxn,i} + \Delta G_{pol,i})\} + \sum_{i=1}^{M} \delta_i \sum_{j=i+1}^{M} \delta_j [\,\Delta G_{ij}] \quad (1)$$

where the summation is over the total *M* conformers of all residues in the protein; for each conformer *i*, δ_i) 1 if it is present in the current microstate *n* and 0 if it is not. Each residue has one conformer with δ_i) 1 and the rest δ_i) 0. In the double summation δ_i and δ_j are both 1 only when conformer *i* and *j* are from two different residues. k_bT is 0.59 kcal/mol (25.8 meV), and m_i is 1 for bases, −1 for acids, and 0 for polar groups and waters. n_i is the number of electrons gained or lost compared to the ground state conformer. For example, if an oxidized conformer is defined as the ground state, it has $n_i = 0$ and the reduced conformer has $n_i = 1$; *F* is the Faraday constant. $pK_{sol,i}$ is the pK_a and $E_{m,sol}$,*i* the midpoint potential of the *i*th cofactor in solution. $\Delta\Delta G_{rxn,i}$ is the difference between the conformer reaction field energy in solution and in the protein (desolvation energy). $\Delta G_{pol,i}$ is the pairwise electrostatic and nonelectro-static interaction of the conformer with the backbone and with side chains that have no conformational degrees of freedom. The torsion energy for each conformer is added to $\Delta G_{pol,i}$. ΔG_{ij} is the electrostatic and Lennard-Jones pairwise interaction between each pair of conformers in the microstate. The limits on the summation of the interconformer terms ensure that each interaction is counted once. Monte Carlo sampling establishes the Boltzmann distribution of the different conformers of each residue at 25 °C. Residue pK_as and E_ms are determined from the fraction group ionization in a series of Monte Carlo simulations at different pHs or E_hs (eq 1). Multiflip (76) between closely coupled residues is implemented (63). The SOFT function is not used (56). For pK_a calculations the heme is fixed in its oxidized state, and the probability of residue protonation, including that of the aquo–heme, is determined as a function of pH (56). For E_m calculations the pH is fixed at 7 and the E_h varied. All groups are allowed to sample different protonation states throughout the heme titration.

Analysis of the MCCE pK_as and E_ms

The E_m or pK_a changes on moving a group from solution to its position in the protein. Thus

$$pK_a = pK_{a,sol} - m\Delta\Delta G_{protein} \quad (2)$$

where pK_a is the group pK_a in the protein, *m* is −1 for an acid and +1 for a base, and

$$E_m = E_{m,sol} - \Delta\Delta G_{protein}/nF \quad (3)$$

where E_m is the heme in situ E_m and n is the number of electrons. The shift in energy of ionization ($\Delta\Delta G_{protein}$) is due to different changes of the reaction reactant and product energies when the reaction is moved into the protein. This term can be broken down in MCCE into the sum:

$$\Delta\Delta G_{protein} = (\Delta\Delta G_{rxn} + \Delta G_{pol}) + \Delta G_{res} \quad (4)$$

including the change in reaction field energy from solution ($\Delta\Delta G_{rxn}$), the added interaction with the rigid backbone (ΔG_{pol}), and the side chains in their ionization and conformation states equilibrated at the given pH and E_h (ΔG_{res}) (20,43,77).

MCCE uses continuum electrostatics to calculate the interaction between the aquo–heme and charges and dipoles in the protein. Selected interactions with the ferric heme porphyrin together with its imidazole and water or hydroxyl ligand were also calculated using Gaussian 98 (67). The heme and imidazole are taken from the crystal structure of sperm whale myoglobin (1A6K), with water or hydroxyl added in GaussView (67). Each structure is then optimized using the B3LYP method (66) with the LANL2DZ basis set (78). Hydroxyl–hemes are expected to be low spin (53,79) while water–hemes are generally high spin (53,80). The water–heme is given a net charge +1 and spin $5/_2$, while the hydroxyl–heme has a net charge 0 and spin $1/_2$. The change in system energy is then calculated with an external charge of +1 or −1 placed next to the aquo–heme complex in positions shown in Figure 1. All atoms are fixed in the structure optimized before the charge is added.

Nine external charges are placed on a plane parallel to the porphyrin plane located 4, 6, 8, 10, or 12 Å from the heme (Figure 1). Points that overlap the water or imidazole ligand are removed. The interactions are also calculated with Coulomb's law with the metal-centered charges used in the MCCE calculations with $\varepsilon = 1$. For the ferric hydroxyl–heme, Coulomb's law reproduces the DFT interactions with an error of <10% and a slope of 0.94 with the exception of points within 4 Å of the heme plane (Figure 2). However, for the water–heme, the Coulomb's law interactions with the points above the heme plane are significantly larger than those obtained with DFT. In contrast, for charges on the heme edge (Figure 1) the Coulomb's law interactions reproduce the DFT interactions with <5% error and a slope of 1.0 for both water and hydroxyl ligated hemes (Figure 2). The source of the error in the CE calculation is not known. However, the large unfavorable interactions with water–heme are relaxed in the DFT calculations, while the smaller, favorable interactions with hydroxyl–heme are not. This suggests that there is significantly more polarization of the ferric water–heme by the external charge. In addition, the correction could be needed if there is significant charge at positions that are not well described by the atom-centered charges used here. Further studies are in progress to develop a water–heme charge distribution, perhaps including charges out of the heme plane, which can better reproduce the DFT interaction with Coulomb's law. Preliminary calculations show that in general there is no systematic error in the CE calculations of the interactions of the standard amino acids with external charges.

The ferric water–heme interaction of a simple external charge at the position of Arg 38 in peroxidase or CuB in oxidase calculated with DFT is only 60% of that found with Coulomb's law. The interaction with a charge at the position of Arg 99 in hemoglobin I is 65% as large. The influence of the charge distribution for the external group on the correction was examined by using a PARSE Arg charge distribution, rather than a single +1 charge. The DFT interaction

is now 63% of that found with Coulomb's law, very similar to that found with a unitary charge model. The influence of the charge distribution of CuB is more complex and cannot be described by a simple scaling factor. The details are discussed in ref 43.

Corrections are applied to interactions of the water–heme with Arg 99 in hemoglobin, Arg 38 in peroxidase, and CuB in oxidase. However, pairwise electrostatic interactions in MCCE are calculated with the Poisson–Boltzmann equation (PB), a CE analysis which takes into account the different dielectric constants of the protein and water (30,81). The scaling factor derived for particular heme–residue geometry from the comparison of Coulomb's law and DFT interactions in a vacuum (Figure 2) is used to scale the individual PB interactions in MCCE. Corrections used for CuB can be found in ref 43.

Interactions with residues that are on the heme plane or far away from the heme are shown to need no correction. Residues that have significant interactions with the aquo–heme which are not corrected because of their position include the following: all of the heme propionates; Arg 45 which is hydrogen bonded to a propionic acid in myoglobin; Lys 179 which is hydrogen bonded to a propionate in hemoglobin 1; Arg 136 and Asp 140 which form an ion pair on the porphyrin edge furthest from the propionates in hemoglobin 1 (Figure 4).

RESULTS AND DISCUSSION

The ferric aquo–heme pK_as were calculated with MCCE in myoglobins from sperm whale and *Aplysia*, hemoglobin I, heme oxygenase 1, horseradish peroxidase, and cytochrome *c* oxidase and compared to measured values. These pK_as span 3.3 pH units from 7.6 in heme oxygenase 1 to 10.9 in the peroxidase. Two sets of calculations are presented. In the first set, standard Poisson–Boltzmann continuum electrostatics (CE) calculations are used for all pairwise interactions between the aquo–heme and the surrounding protein residues. In the second, an additional correction derived from DFT calculations is applied. Calculated pK_as are compared to the experimental values. Calculations of the heme E_ms are discussed below.

The pK_as calculated using the standard CE-based pairwise interactions in MCCE (20) do not provide consistent agreement with the experimental data (Figure 3). Calculated pK_as for the myoglobins and heme oxygenase are within 1 pH unit of the measured values. However, errors as large as 6 pH units are found in horseradish peroxidase and cytochrome *c* oxidase. In these proteins a nearby positive charge in the heme distal pocket lowers the calculated pK_a, while the myoglobins have no charges in similar positions. As described in the Methods section CE and DFT calculations provide very similar values for pairwise interactions between a charge and a neutral hydroxyl–heme, probably because the electronic polarization does not contribute much to this smaller, favorable interaction. For the cationic water–heme, both methods also yield similar results when the charge is on the heme edge. However, when the charge is above the heme plane near the iron, the interactions derived with a CE analysis are significantly larger than those obtained with DFT calculations. The closer the charge is to the heme plane, the larger the discrepancy (Figure 2). The large unfavorable interactions are relaxed when electronic polarization is considered in the DFT calculations. The DFT corrections are applied to the pairwise electrostatic interaction of the water–heme with Arg 99 in hemoglobin I, Arg 38 in horseradish peroxidase, and CuB in cytochrome *c* oxidase to recalculate the pK_as. Now calculated pK_as in the six proteins agree with the measured values within 1 pH unit. Analysis of the MCCE calculations can then show how interactions and conformational changes shift the p$K_{a,sol}$ of 9.6 to different in situ values in these proteins.

Sperm Whale Myoglobin

Sperm whale myoglobin has a folded six-helix core (Figure 4). The pK_a of the ferric aquo–heme is 8.95 (52), little different from the p$K_{a,sol}$ of 9.6. MCCE calculations with seven

different crystal structures give an average aquo–heme pK_a of 9.1 (1.0, in good agreement with experiment. This heme is close to the protein surface. However, p$K_a \approx$ p$K_{a,sol}$ not because the heme does not interact with the protein but rather because a number of effects cancel (Table 1). The water–heme, with a net +1 charge, has 7 ΔpK units (9.52 kcal/mol) less solvation energy in the protein than it does in water, but the hydroxyl–heme, which has a large dipole moment, has a 5 ΔpK unit desolvation energy. Thus, the resultant desolvation penalty ($\Delta\Delta G_{rxn}$) favors the water–heme complex raising the pK_a by about 2 pH units. The backbone amide dipoles tend to raise the electrostatic potential within all proteins, shifting residue pK_as (25,82) and cytochrome E_ms (20). Here they favor the hydroxyl–heme, lowering the pK_a by 1 pH unit. The E helix, which contains His 64 in the distal pocket, is the largest contributor.

There are 4 Arg, 14 Glu, 7 Asp, and 19 Lys in the protein and all of them are >95% ionized between pH 7 and pH 9. However, most of these charges have little effect on the aquo–heme pK_a because they are solvent exposed. Arg 45, which is hydrogen-bonded to the D-ring propionic acid, does shift the pK_a down by 0.6 pK unit (propionate A and D designated as assigned in the PDB structure files). The two heme propionic acids are both fully ionized and together shift the pK_a up by 2.3 units. As these are all near the heme edge, the CE interaction agrees with the DFT values (Figure 2). His 64 in the distal heme pocket near the aquo–ligand undergoes a conformational change with the change in the aquo–heme protonation state (Figure 4). The His is always neutral, but the δ proton tautomer stabilizes the positive water–heme by 3–4 ΔpK units, while the protonated ε tautomer stabilizes the hydroxyl–heme by 1.6–2.5 ΔpK units. In different PDB structures the His tautomer is restricted by the rigid backbone to different extents, yielding the dependence of the calculated pK_a on the starting structure. Arg 45 not only lowers the aquo–heme pK_a by direct electrostatic interaction but it also lowers the pK_a indirectly by favoring the εHis 64 conformer.

Aplysia Myoglobin

Myoglobin from the sea hare *Aplysia limacine* has a folded six-helix structure (Figure 4). It is calculated to have a ferric aquo–heme pK_a of 7.7, 2 pK units lower than that of sperm whale myoglobin, in agreement with the experimental value of 7.6 (52). The *Aplysia* and sperm whale proteins have the same protein folds and are 27% identical. The analogue of myoglobin His 64 is Val 64 in the *Aplysia* distal pocket, providing a bigger cavity, so the heme is slightly better solvated, shifting the pK_a up. However, the biggest difference between the two proteins is in ΔG_{res}. The loss of His 64 and protonation of the ring D propionic acid lowers the aquo–heme pK_a. The propionate pK_a is raised to 8.6 by the nearby Asp 45, while in myoglobin Arg 45 lowers the propionate pK_a to 4.6.

Hemoglobin I

Monomeric clam hemoglobin I also has a folded six-helix structure (Figure 4). The aquo–heme pK_a is calculated to be 9.8 and measured to be 9.6 (83), close to that of sperm whale myoglobin. The hemoglobin I and myoglobin have similar structures with 23% identity. A larger cavity in the heme distal pocket leads to a smaller desolvation energy. As His 64 does in myoglobin, Gln 64 changes conformation, keeping its oxygen pointing toward the water–heme and nitrogen pointing toward the hydroxyl–heme. Arg 99, on the proximal side of the heme, shifts the pK_a down by 1.5 pH units, while the two propionic acids, both of which are ionized, shift the pK_a up by 2.2 pH units.

Heme Oxygenase 1

Rat heme oxygenase 1 is a multihelical bundle with two three-helix motifs (Figure 4). The aquo–heme pK_a is calculated to be 7.5, in agreement with the experimental value of 7.6 (84, 85). In this protein heme is an exchangeable substrate and is significantly more exposed than in the other proteins considered here and so has a very small $\Delta\Delta G_{rxn}$. The large positive

potential from the backbone lowers the pK_a by 3.3 pH units. The distal pocket helix is kinked at Gly 143 and Gly 144 so the backbone amides of Ser 142, Gly 143, and Gly 144 all point toward the heme iron, stabilizing the hydroxyl–heme. Arg 136 and Asp 140 are in a salt bridge near the porphyrin edge. While each interacts with the aquo–heme by over 3 Δp*K* units, their combined impact is small.

Horseradish Peroxidase

The multihelical peroxidase uses heme to reduce hydrogen peroxide to water. The aquo–heme pK_a is calculated to be 10.1, in reasonable agreement with the measured 10.9 (52). The aquo–heme has a similar reaction field energy loss as the globins. Unlike the globins, interactions with the backbone amides near the metal center are small and somewhat negative, raising the pK_a by 0.6 pH unit. Interactions with other residues raise the pK_a by 1.5 Δp*K* units. His 42 and Asp 43 raise the pK_a by 6 pH units while Arg 38 shifts the pK_a down by 4.5 pH units (assuming a 60% DFT correction). His 42 sits in the distal pocket in a position similar to His 42 in myoglobin. However, this His is fixed in the δ tautomer by Arg 38, Glu 64, and Asn 70, stabilizing the protonated water–heme.

Cytochrome c Oxidase

Heme *a*3 in cytochrome *c* oxidase is deeply buried in the transmembrane 12-helix subunit I of the protein. In the mixed-valence state, with heme *a* and CuB reduced, the ferric aquo–heme pK_a has been measured to be 9 (53). Using the full CE interaction between CuB and the aquo–heme, the calculated pK_a is 3. The DFT correction reduces the interaction from 6.4 to 3.2 Δp*K* units. Since the aquo–heme titration now occurs at higher pH, the protein net charge is more negative than when the titration is at pH 3. This raises the pK_a further to 8.6, in good agreement with experiment (43). The cytochrome *c* oxidase heme is more deeply buried than in the other proteins, losing more reaction field energy, which shifts the pK_a down. Within the membrane-embedded protein, pairwise electrostatic interactions with other residues are quite long range. However, the net interaction of the fully ionized propionic acids and the rest of the protein shifts the pK_a up by only 2 pH units.

E_m Calculations

The aquo–heme E_ms were calculated in each protein at pH 7. E_ms previously measured in four of the proteins range from −250 mV in peroxidase to 125 mV in *Aplysia* myoglobin (86) (Table 1b). MCCE calculations agree with the experimental values with errors of e35 mV. MCCE allows protonation of the aquo–heme to be coupled to heme reduction (20). The relevant $E_{m,sol}$ for water–heme of −120 mV (72,73) and for hydroxyl–heme of −200 mV (72) is included in the microstate energy (eq 1) so the pH dependence of the E_m is properly treated in the redox titration. This degree of freedom could be important for *Aplysia* myoglobin and heme oxygenase, which have pK_as near 7. However, since their ferric pK_as are above 7 and ferrous pK_as are higher, the aquo–heme ligand remains predominately water at pH 7.

Electrostatic interactions that favor the ferric heme with its net charge of +1 over the neutral ferrous heme shift the E_m down. The same electrostatic interactions favor the cationic ferric water–heme over the neutral hydroxyl–heme, raising the pK_a. While a higher pK_a is correlated with a lower E_m, the connection is by no means exact (Figure 5). In most proteins, the $\Delta\Delta G_{protein}$ for the redox reaction is larger than for the protonation reaction so the E_m is shifted from $E_{m,sol}$ by more than the pK_a is shifted from p$K_{a,sol}$ (Figure 5, eqs 2 and 3). One difference is the desolvation energy is on average 2.4 ± 0.3 Δp*K* units larger for the redox reaction than for the protonation reaction (Table 1). Because of its significant dipole the solvated neutral ferric hydroxyl–heme has a solvation energy that is not much smaller than the positively charged ferric water–heme. Thus, both reactant and product of the protonation reaction have similar $\Delta\Delta G_{rxn}$. With the exception of cytochrome *c* oxidase, the desolvation penalty, which

always favors the neutral species, shifts the pK_a down by at most 2 pH units. In contrast, when compared to the neutral, ferrous water–heme, the cationic, ferric water–heme has much larger interactions with water. The impact of the desolvation energy on the redox reaction when the heme is buried in the protein is thus much larger.

Hemoglobin I has a pK_a which is only 0.2 pH unit higher than the p$K_{a,sol}$, while the E_m is 223 mV more positive than $E_{m,sol}$ ($\Delta\Delta G_{protein}$ = 3.8 ΔpK units). The difference in desolvation energy for the two reactions contributes 3 ΔpK units. In addition, Gln 64 in the distal pocket changes conformation in the aquo–heme pK_a titration but does not in the E_m titration. The rigid Gln 64 raises the water–heme E_m by 1 ΔpK unit (58 meV) more than it shifts the ferric aquo–heme pK_a down. The reorientation of the Gln is part of the protein dielectric response that is captured by the explicit motions available in MCCE (30,55). The Gln motion coupled to aquo–heme protonation thus diminishes the effective pairwise interaction.

In horseradish peroxidase, $\Delta\Delta G_{protein}$ shifts the E_m down more than it shifts the pK_a up. Besides the 2.2 ΔpK unit difference in the desolvation energy, ΔG_{res} favors heme reduction 3.3 ΔpK units more than water deprotonation. Although both ferrous water–heme and ferric hydroxyl–heme have a net charge of 0, they interact differently with nearby residues. The hydroxyl–heme has a large dipole with its negatively charged hydroxide pointing toward the distal pocket. Arg 38 in the distal pocket and Asp 247 on the opposite side form a dipole stabilizing the hydroxyl–heme. The difference in interactions with hydroxyl–heme and water–heme is relatively small, leading to a small ΔG_{res}, contributing to the pK_a shift. On the other hand, the neutral ferrous water–heme is not stabilized by the electrostatic dipole generated by these two amino acids while interactions of the ferric water–heme with nearby negative charges shift the E_m down.

As in horseradish peroxidase, the favorable interaction of CuB with the hydroxyl–heme in cytochrome *c* oxidase makes the contribution of ΔG_{res} to the in situ pK_a smaller than found for in situ E_m. Assuming the $E_{m,sol}$ of heme a is 100 (1) to 160 (74,75) mV more positive than that of heme c, the E_m of heme a3 is predicted to be 9 to 69 mV in cytochrome *c* oxidase when CuA is oxidized and heme A and CuB are reduced.

There are no experimental data available for the E_m in heme oxygenase 1. These calculations predict an E_m of 40 mV. A run of four backbone dipoles lowers the pK_a more than the E_m. All of the other proteins studied here have similar values of ΔG_{pol} for the redox and protonation reactions.

CONCLUSIONS

The pK_as of ferric aquo–heme at pH 7 in sperm whale myoglobin, *Aplysia* myoglobin, hemoglobin I, heme oxygenase 1, horseradish peroxidase, and cytochrome *c* oxidase were calculated with MCCE. The calculations reveal a breakdown in the classic continuum electrostatic analysis of pairwise interactions. Large errors in calculated pK_as were found in horseradish peroxidase and cytochrome *c* oxidase. DFT calculations suggest that CE calculations overestimate pairwise interactions between ferric water–heme and a positive charge above the heme plane. This could be due to significant out-of-plane charge density, which would be ignored in the atom-centered charges used in the CE analysis. Alternatively, these external charges could polarize ferric hydroxyl–heme significantly more than the amount accounted for by the ε = 4 used in the MCCE calculation. Using a correction that brings the DFT and CE interactions into agreement, the calculated pK_as in six proteins are within 1 pH unit of the experimental values. The calculated E_ms using the correction derived from DFT calculations are within 35 mV of the experimental values.

Proteins with higher ferric aquo–heme pK_as have lower E_ms since both arise from the protein stabilizing a positively charged heme. However, the proteins shift the free energy of the redox

reaction ($\Delta\Delta G_{protein}$) by an amount that would shift a pK_a by >6 pH units (375 mV), while the pK_as span only 3.3 pH units (eqs 2 and 3). The difference in $\Delta\Delta G_{protein}$ shows that there is a larger effective dielectric response for the protonation than the redox reactions. In sperm whale myoglobin and hemoglobin I protonation is coupled to conformational changes while the redox reaction is not. These conformation changes allow a residue in the distal pocket to stabilize both protonation states, reducing the energy difference between them. In contrast, when the group is rigid as it is for the redox reaction, the pairwise interactions are larger, shifting the E_m more. This difference in flexibility for the two reaction types found in MCCE is supported by the good match between calculation and experiment for both pK_as and E_ms.

Supplementary Material

Refer to Web version on PubMed Central for supplementary material.

Acknowledgments

We gratefully acknowledge helpful discussions with Ronald Koder.

References

1. Reedy CJ, Gibney BR. Heme protein assemblies. Chem Rev 2004;104:617–649. [PubMed: 14871137]
2. Antonin, E.; Brunori, M. Hemoglobin and Myoglobin in their Reactions with Ligands. North-Holland, Amsterdam: 1971.
3. Tenhunen R, Marver HS, Schmid R. Microsomal heme oxygenase. Characterization of the enzyme. J Biol Chem 1969;244:6388–6394. [PubMed: 4390967]
4. Welinder KG. Superfamily of plant, fungal and bacterial peroxidases. Curr Opin Struct Biol 1992;2:338–393.
5. Smith AT, Veitch NC. Substrate binding and catalysis in heme peroxidases. Curr Opin Chem Biol 1998;2:269–278. [PubMed: 9667928]
6. Brzezinski P. Redox-driven membrane-bound proton pumps. Trends Biochem Sci 2004;29:380–387. [PubMed: 15236746]
7. Gennis RB. Some recent contributions of FTIR difference spectroscopy to the study of cytochrome oxidas. FEBS Lett 2003;555:2–7. [PubMed: 14630310]
8. Ferguson-Miller S, Babcock GT. Heme/copper terminal oxidases. Chem Rev 1996;96:2889–2907. [PubMed: 11848844]
9. Wikstrom M. Cytochrome *c* oxidase: 25 years of the elusive proton pump. Biochim Biophys Acta 2004;1655:241–247. [PubMed: 15100038]
10. Montfort WR, Weichsel A, Andersen JF. Nitrophorins and related antihemostatic lipocalins from Rhodnius prolixus and other blood-sucking arthropods. Biochim Biophys Acta 2000;1482:110–118. [PubMed: 11058753]
11. Privalle CT, Crivello JF, Jefcoate CR. Regulation of intramitochondrial cholesterol transfer to side-chain cleavage cytochrome P-450 in rat adrenal gland. Proc Natl Acad Sci USA 1983;80:702–706. [PubMed: 6298770]
12. Pikuleva I, Waterman M. Cytochromes P450 in synthesis of steroid hormones, bile acids, vitamin D3 and cholesterol. Mol Aspects Med 1999;20:33–42. 43–37. [PubMed: 10575650]
13. Rodgers KR. Heme-based sensors in biological systems. Curr Opin Chem Biol 1999;3:158–167. [PubMed: 10226051]
14. Chan MK. Recent advances in heme-protein sensors. Curr Opin Struct Biol 2001;5:216–222.
15. Churg AK, Warshel A. Control of the redox potential of cytochrome *c* and microscopic dielectric effects in proteins. Biochemistry 1986;25:1675–1681. [PubMed: 3011070]
16. Poulos TL. Heme enzyme crystal structure. Heme Proteins: Struct Funct, Genet 1988;7:2–36.
17. Rietjens I. The role of the axial ligand in heme-based catalysis. J Biol Inorg Chem 1996;1:355.

18. Martin ACR, Orengo CA, Hutchinson EG, Jones S, Karmirantzou M, Laskowski RA, Mitchell JBO, Taroni C, Thornton JM. Protein folds and function. Structure 1998;6:875–884. [PubMed: 9687369]
19. Stellwagen E. Haem exposure as the determinate of oxidation–reduction potential of haem proteins. Nature 1978;275:73–74. [PubMed: 683346]
20. Mao J, Hauser K, Gunner MR. How cytochromes with different folds control heme redox potentials. Biochemistry 2003;42:9829–9840. [PubMed: 12924932]
21. Gunner MR, Honig B. Electrostatic control of midpoint potentials in the cytochrome subunit of the *Rhodopseudomonas viridis* reaction center. Proc Natl Acad Sci USA 1991;88:9151–9155. [PubMed: 1924378]
22. Voigt P, Knapp EW. Tuning heme redox potentials in the cytochrome *c* subunit of photosynthetic reaction centers. J Biol Chem 2003;278:51993–52001. [PubMed: 12975370]
23. Kassner RJ. A theoretical model for the effects of local nonpolar heme environments on the redox potentials in cytochromes. J Am Chem Soc 1973;95:7959–7975.
24. Kassner RJ. Effects of nonpolar environments on the redox potentials of heme complexes. Proc Natl Acad Sci USA 1972;69:2263–2267. [PubMed: 4506096]
25. Kim J, Mao J, Gunner MR. Are acidic and basic groups in buried proteins predicted to be ionized? J Mol Biol 2005;348:1283–1298. [PubMed: 15854661]
26. Muegge I, Qi PX, Wand AJW, Chu ZT, Warshel A. The reorganization energy of cytochrome *c* revisted. J Phys Chem 1997;101:825–836.
27. Churg AK, Weiss RM, Warshel A, Takano T. On the action of cytochrome *c*: correlating geometry changes upon oxidation with activation energies of electron transfer. J Phys Chem 1983;87:1683–1694.
28. Cutler RL, Davies AM, Creighton S, Warshel A, Moore GR, Smith M, Mauk AG. Role of arginine-38 in regulation of the cytochrome *c* oxidation–reduction equilibrium. Biochemistry 1989;28:3188–3197. [PubMed: 2545252]
29. Warwicker J, Watson HC. Calculation of the electric potential in the active site cleft due to a α-helix dipoles. J Mol Biol 1982;157:671–679. [PubMed: 6288964]
30. Gunner MR, Alexov E. A pragmatic approach to structure based calculation of coupled proton and electron transfer in proteins. Biochim Biophys Acta 2000;1458:63–87. [PubMed: 10812025]
31. Zhou HX. Control of reduction potential by protein matrix: lesson from a spherical protein model. J Biol Inorg Chem 1997;2:109–113.
32. Warshel A, Papazyan A, Muegge I. Microscopic and semimacroscopic redox calculations: what can and can not be learned from continuum models. J Biol Inorg Chem 1997;2:143–152.
33. Baptista AM, Martel PJ, Peterson SB. Simulation of protein conformational freedom as a function of pH: constant-pH molecular dynamics using implicit titration. Proteins: Struct Funct, Genet 1997;27:523–544. [PubMed: 9141133]
34. Soares CM, Martel PJ, Mendes J, Carrondo MA. Molecular dynamics simulation of cytochrome c_3: studying the reduction processes using free energy calculations. Biophys J 1998;74:1708–1721. [PubMed: 9545034]
35. Baptista A, Martel PJ, Soares CM. Simulation of electron-proton coupling with a Monte Carlo method: application to cytochrome c_3 using continuum electrostatics. Biophys J 1999;76:2978–2998. [PubMed: 10354425]
36. Martel PJ, Soares CM, Baptista AM, Fuxreiter M, Naray-Szabo G, Louro RO, Carrondo MA. Comparative redox and pK_a calculations on cytochrome *c*3 from several *DesulfoVibrio* species using continuum electrostatic methods. J Biol Inorg Chem 1999;4:73–86. [PubMed: 10499105]
37. Zaric SD, Popovic DM, Knapp EW. Factors determining the orientation of axially coordinated imidazoles in heme proteins. Biochemistry 2001;40:7914–7928. [PubMed: 11425320]
38. Haas AH, Lancaster CR. Calculated coupling of transmembrane electron and proton transfer in dihemic quinol: fumarate reductase. Biophys J 2004;87:4298–4315. [PubMed: 15361415]
39. Rogers NK, Moore GR, Sternberg MJE. Electrostatic interactions in globular proteins: Calculation of the pH dependence of the redox potential of cytochrome c_{551}. J Mol Biol 1985;182:613–616. [PubMed: 2989537]

40. Rogers NK, Moore GR. On the energetics of conformational changes and pH dependent redox behaviour of electron transfer proteins. FEBS Lett 1988;228:69–73. [PubMed: 2830136]
41. Kannt A, Lancaster CRD, Michel H. The coupling of electron transfer and proton translocation: electrostatic calculations on *Paracoccus denitrificans* cytochrome *c* oxidase. Biophys J 1998;74:708–721. [PubMed: 9533684]
42. Popovic DM, Stuchebrukhov AA. Electrostatic study of the proton pumping mechanism in bovine heart cytochrome *c* oxidase. J Am Chem Soc 2004;126:1858–1871. [PubMed: 14871119]
43. Song Y, Michonova-Alexova E, Gunner MR. Calculated proton uptake on anaerobic reduction of cytochrome c oxidase: Is the reaction electroneutral? Biochemistry 2006;45:XXXX–XXXX.
44. Siegbahn PE. The catalytic cycle of tyrosinase: peroxide attack on the phenolate ring followed by O–O cleavage. J Biol Inorg Chem 2003;8:567–576. [PubMed: 12634912]
45. Green MT. Role of the axial ligand in determining the spin state of resting cytochrome P450. J Am Chem Soc 1998;120:10772–10773.
46. Guallar V, Friesner RA. Cytochrome P450CAM enzymatic catalysis cycle: a quantum mechanics/molecular mechanics study. J Am Chem Soc 2004;126:8501–8508. [PubMed: 15238007]
47. Schoneboom JC, Thiel W. The resting state of $P450_{cam}$: A QM/MM study. J Phys Chem B 2004;108:7468–7478.
48. Ogliaro F, Harris N, Cohen S, Filatov M, deVisser DP, Shaik S. A model "rebound" mechanism of hydroxylation by cytochrome P450: Stepwise and effectively conderted pathways and their reactivity patterns. J Am Chem Soc 2000;122:8977–8989.
49. Kamachi T, Yoshizawa K. A theoretical study on the mechanism of camphor hydroxylation by compound I of cytochrome P450. J Am Chem Soc 2003;125:4652–4661. [PubMed: 12683838]
50. Guallar V, Baik MH, Lippard SJ, Friesner RA. Peripheral heme substituents control the hydrogen-atom abstraction chemistry in cytochromes P450. Proc Natl Acad Sci USA 2003;100:6998–7002. [PubMed: 12771375]
51. Schoneboom JC, Cohen S, Lin H, Shaik S, Thiel W. Quantum mechanical/molecular mechanical investigation of the mechanism of C–H hydroxylation of camphor by cyto-chrome P450cam: theory supports a two-state rebound mechanism. J Am Chem Soc 2004;126:4017–4034. [PubMed: 15038756]
52. Brunori M, Amiconi G, Antonin E, Wyman J, Zito R, Fanelli AR. The transition between "acid" and "alkaline" ferric heme proteins. Biochim Biophys Acta 1968;154:315–322. [PubMed: 5637052]
53. Branden M, Namslauer A, Hansson O, Aasa R, Brzezinski P. Water-hydroxide exchange reactions at the catalytic site of heme-copper oxidases. Biochemistry 2003;42:13178–13184. [PubMed: 14609328]
54. Berman HM, Westbrook J, Feng Z, Gilliland G, Bhat TN, Weissig H, Shindyalov IN, Bourne PE. The protein data bank. Nucleic Acids Res 2000;28:235–242. [PubMed: 10592235]
55. Alexov EG, Gunner MR. Incorporating protein conformational flexibility into the calculation of pH-dependent protein properties. Biophys J 1997;72:2075–2093. [PubMed: 9129810]
56. Georgescu RE, Alexov EG, Gunner MR. Combining conformational flexibility and continuum electrostatics for calculating pK_as in proteins. Biophys J 2002;83:1731–1748. [PubMed: 12324397]
57. Gunner MR, Mao J, Song Y, Kim J. Factors influencing energetics of electron and proton transfers in proteins. What can be learned from calculations. Biochim Biophys Acta. 2006in press
58. Nicholls A, Honig B. A rapid finite difference algorithm utilizing successive over-relaxation to solve the Poisson–Boltzmann equation. J Comput Chem 1991;12:435–445.
59. Bharadwaj R, Windemuth A, Sridharan S, Honig B, Nicholls A. The fast multipole boundary element method for molecular electrostatics: An optimal approach for large systems. J Comput Chem 1995;16:898–913.
60. Rocchia W, Alexov E, Honig B. Extending the applicability of the nonlinear Poisson–Boltzmann equation: multiple dielectric constants and multivalent ions. J Phys Chem B 2001;105:6507–6514.
61. Gilson MK, Honig B. Calculation of the total electrostatic energy of a macromolecular system: solvation energies, binding energies, and conformational analysis. Proteins: Struct Funct, Genet 1988;4:7–18. [PubMed: 3186692]

62. Sitkoff D, Sharp KA, Honig B. Accurate calculation of hydration free energies using macroscopic solvent models. J Phys Chem 1994;98:1978–1988.
63. Song Y, Mao J, Gunner MR. Calculation of proton transfers in bacteriorhodopsin bR and M intermediates. Biochemistry 2003;42:9875–9888. [PubMed: 12924936]
64. Cornell WD, Cieplak P, Bayly CI, Gould IR, Merz JKM, Ferguson DM, Spellman DC, Fox T, Caldwell JW, Kollman PA. A second generation force field for the simulation of proteins, nucleic acids, and organic molecules. J Am Chem Soc 1995;117:5179–5197.
65. Mao J, Song Y, Gunner MR. Better rotamer packing for continuum electrostatics pK_a calculations: MCCE2. J Comput Chem. 2006in preparation
66. Becke AD. Density-Functional Thermochemistry. 3 The role of exact exchange. J Chem Phys 1993;98:5648–5652.
67. Frisch, MJ.; Trucks, GW.; Schlegel, HB.; Scuseria, GE.; Robb, MA.; Cheeseman, JR.; Zakrzewski, VGJA.; Montgomery, J.; Stratmann, RE.; Burant, JC.; Dapprich, S.; Millam, JM.; Daniels, AD.; Kudin, KN.; Strain, MC.; Farkas, O.; Tomasi, J.; Barone, V.; Cossi, M.; Cammi, R.; Mennucci, B.; Pomelli, C.; Adamo, C.; Clifford, S.; Ochterski, J.; Petersson, GA.; Ayala, PY.; Cui, Q.; Morokuma, K.; Malick, DK.; Rabuck, AD.; Raghavachari, K.; Foresman, JB.; Cioslowski, J.; Ortiz, JV.; Baboul, AG.; Stefanov, BB.; Liu, G.; Liashenko, A.; Piskorz, P.; Komaromi, I.; Gomperts, R.; Martin, RL.; Fox, DJ.; Keith, T.; Al-Laham, MA.; Peng, CY.; Nanayakkara, A.; Challacombe, M.; Gill, PMW.; Johnson, B.; Chen, W.; Wong, MW.; Andres, JL.; Gonzalez, C.; Head-Gordon, M.; Replogle, ES.; Pople, JA. Gaussian. Vol. 98. Gaussian, Inc; Pittsburgh, PA: 1998. Revision A.9
68. Richarz R, Wüthrich K. Carbon-13 NMR chemical shifts of the common amino acid residues measured in aqueous solutions of the linear tetrapeptides H-Gly-Gly-X-L-Ala-OH. Biopolymers 1975;17:2133–2141.
69. Matthew JB, Gurd FRN, Garcia-Moreno B, Flanagan MA, March KL, Shire SJ. pH-dependent processes in proteins. CRC Crit Rev Biochem 1985;18:91–197. [PubMed: 3899508]
70. Munro OQ, Marques HM. Heme-peptide models for hemoproteins. 1 solution chemistry of *N*-acetylmicroperoxi-dase-8. Inorg Chem 1996;35:3752–3767. [PubMed: 11666562]
71. Vashi PR, Marques HM. The coordination of imidazole and substituted pyridines by the hemeoctapeptide *N*-acetyl-ferromicroperoxidase-8 (Fe^{II}NAcMP8). J Inorg Biochem 2004;98:1471–1482. [PubMed: 15337599]
72. Marques HM, Cukrowski I, Vashi PR. Coordination of weak field ligands by *N*-acetylmicroperoxidase-8 (NAcMP8), a ferric haempeptide from cytochrome *c*, and the influence of the axial ligand on the reduction potential of complexes of NAcMP8. J Chem Soc 2000;2000:1335–1342.
73. Santucci R, Reinhard H, Brunori M. Direct electrochemistry of the undacapeptide from cytochrome *c* (microperoxidase) at a glassy carbon electrode. J Am Chem Soc 1988;110:8536–8357.
74. Vanderkooi G, Stotz E. Reductive alteration of heme a hemochromes. J Biol Chem 1965;240:3418–3424. [PubMed: 14321382]
75. Vanderkooi G, Stotz E. Oxidation–reduction potentials of heme a hemochromes. J Biol Chem 1966;241:3316–3323. [PubMed: 5913120]
76. Beroza P, Fredkin DR, Okamura MY, Feher G. Protonation of interacting residues in a protein by a Monte Carlo method: application to Lysozyme and the photosynthetic reaction center of *Rhodobacter sphaeroides*. Proc Natl Acad Sci USA 1991;88:5804–5808. [PubMed: 2062860]
77. Zhu Z, Gunner MR. Energetics of quinone-dependent electron and proton transfers in *Rhodobacter sphaeroides* photosynthetic reaction centers. Biochemistry 2005;44:82–96. [PubMed: 15628848]
78. Hay PJ, Wadt WR. Ab initio effective core potentials for molecular calculations. Potentials for the transition metal atoms Sc to Hg. J Chem Phys 1985;82:270–283.
79. Sitter AJ, Shifflett JR, Terner J. Resonance Raman spectroscopic evidence for heme iron-hydroxide ligation in peroxidase alkaline forms. J Biol Chem 1988;263:13032–13038. [PubMed: 3417650]
80. Peisach J, Blumberg WE, Ogawa S, Rachmilewitz EA, Oltzik R. The effects of protein conformation on the heme symmetry in high spin ferric heme proteins as studied by electron paramagnetic resonance. J Biol Chem 1971;246:3342–3355. [PubMed: 4324897]
81. Honig B, Nicholls A. Classical electrostatics in biology and chemistry. Science 1995;268:1144–1149. [PubMed: 7761829]

82. Gunner MR, Saleh MA, Cross E, ud-Doula A, Wise M. Backbone dipoles generate positive potentials in all proteins: origins and implications of the effect. Biophys J 2000;78:1126–1144. [PubMed: 10692303]

83. Kraus DW, Wittenberg JB, Lu JF, Peisach J. Hemoglobins of the *Lucina pectinata*/bacteria symbiosis. II An electron paramagnetic resonance and optical spectral study of the ferric proteins. J Biol Chem 1990;265:16054–16059. [PubMed: 2168877]

84. Sun J, Wilks A, Ortiz de Montellano PR, Loehr TM. Resonance Raman and EPR spectroscopic studies on heme–heme oxygenase complexes. Biochemistry 1993;32:14151–14157. [PubMed: 8260499]

85. Takahashi S, Wang J, Rousseau DL, Ishikawa K, Yoshida T, Host JR, Ikeda-Saito M. Heme-heme oxygenase complex. Structure of the catalytic site and its implication for oxygen activation. J Biol Chem 1994;269:1010–1014. [PubMed: 8288555]

86. Taylor JF. Measurement of the oxidation-reduction equilibria of hemoglobin and myoglobin. Methods Enzymol 1981;76:577–582. [PubMed: 7329278]

87. Kraus DW, Wittenberg JB. Hemoglobins of the *Lucina pectinata*/bacteria symbiosis. I Molecular properties, kinetics and equilibria of reactions with ligands. J Biol Chem 1990;265:16043–16053. [PubMed: 2398044]

88. Yamada H, Makino R, Yamazaki I. Effects of 2,4-substituents of deuteropheme upon redox potentials of horseradish peroxidases. Arch Biochem Biophys 1975;169:344–353. [PubMed: 239639]

89. Harbury HA. Oxidation-reduction potentials of horseradish peroxidase. J Biol Chem 1957;225:1009–1024. [PubMed: 13416301]

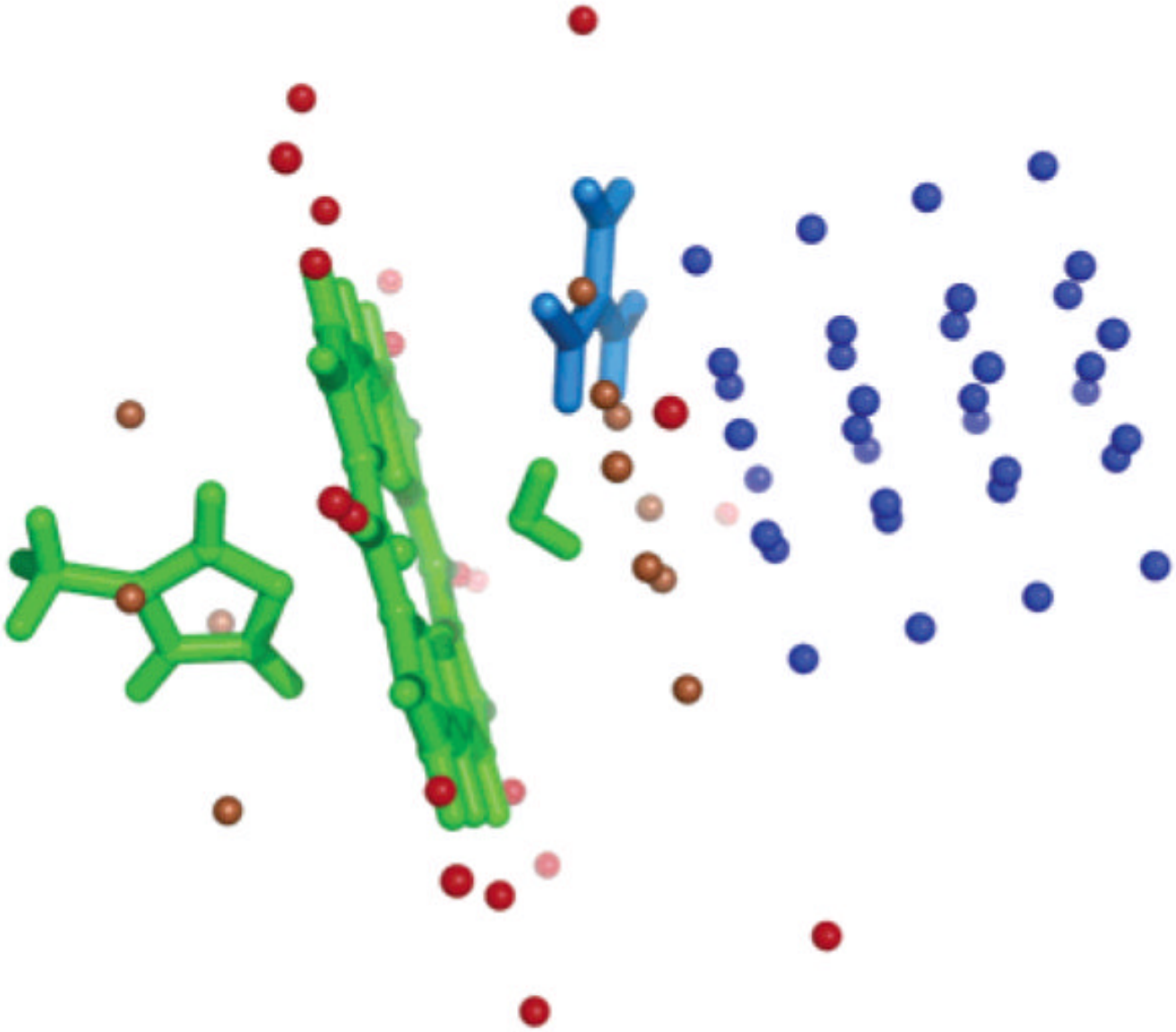

Figure 1.
Position of external charges for comparison of CE and DFT interactions. Blue points are near the heme face; red points are in the plane of the heme and near the heme edge. Those within 4 Å of the heme plane are in brown. His–aquo–heme is in green. The position of Arg 38 in horseradish peroxidase is shown in blue.

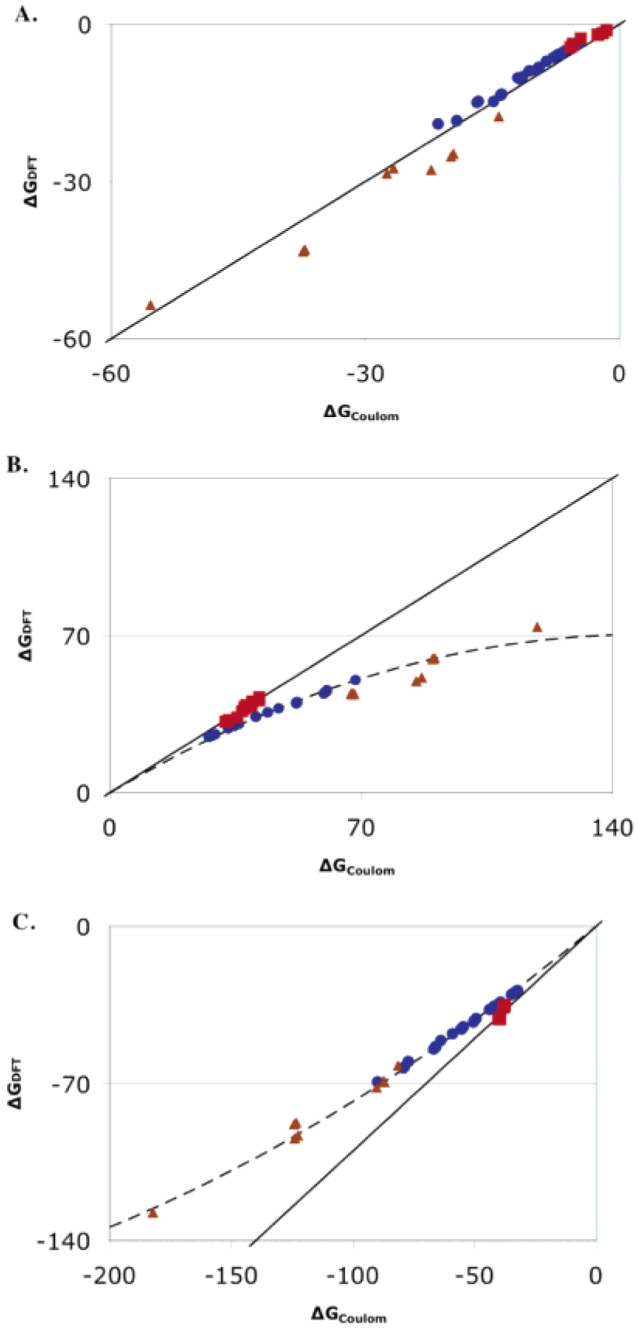

Figure 2.

Comparison of interactions with a positive charge (blue ●) near the heme face, (red ■) in the plane of the heme and near the heme edge, and (brown ▲) within 4 Å of the heme plane as shown in Figure 1 calculated with DFT or CE Coulomb's law with $3\varepsilon = 1$. (A) Neutral, ferric (hydroxyl–heme). The ideal straight line through the origin with a slope of 1 is shown. (B) Cationic, ferric water–heme. The line through the points, $y = 0.95x - (3.2 \times 10^{-3})x^2$, is the best fit to a binomial function for the points near the heme face (blue). (C) (Hydroxyl–heme) – (water–heme). The line through the points is $y = 0.89x + (1.1 \times 10^{-3})x^2$.

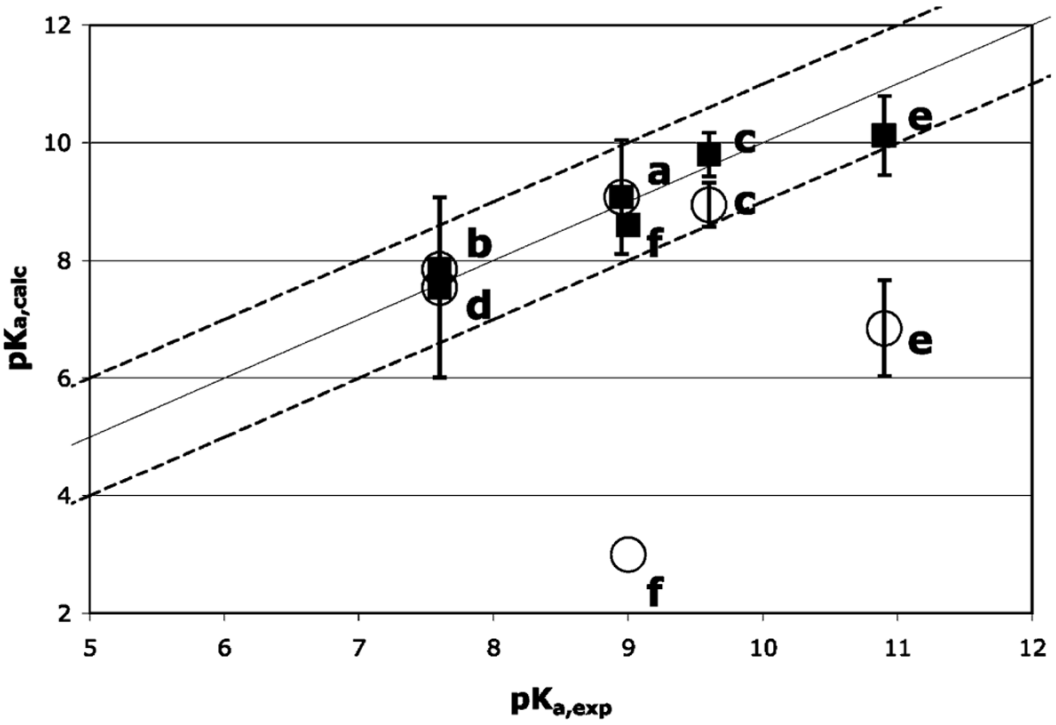

Figure 3.

Comparison of calculated and experimental pK_as (■) with and (○) without the DFT correction for (a) sperm whale myoglobin, (b) *Aplysia* myoglobin, (c) hemoglobin I, (d) heme oxygenase, (e) horseradish peroxidase, and (f) cytochrome *c* oxidase. The ideal line of slope 1 passing through the origin and lines with differences between experimental and calculated of (1 pH unit (dashed lines) are shown. References for experimental values are in Table 1.

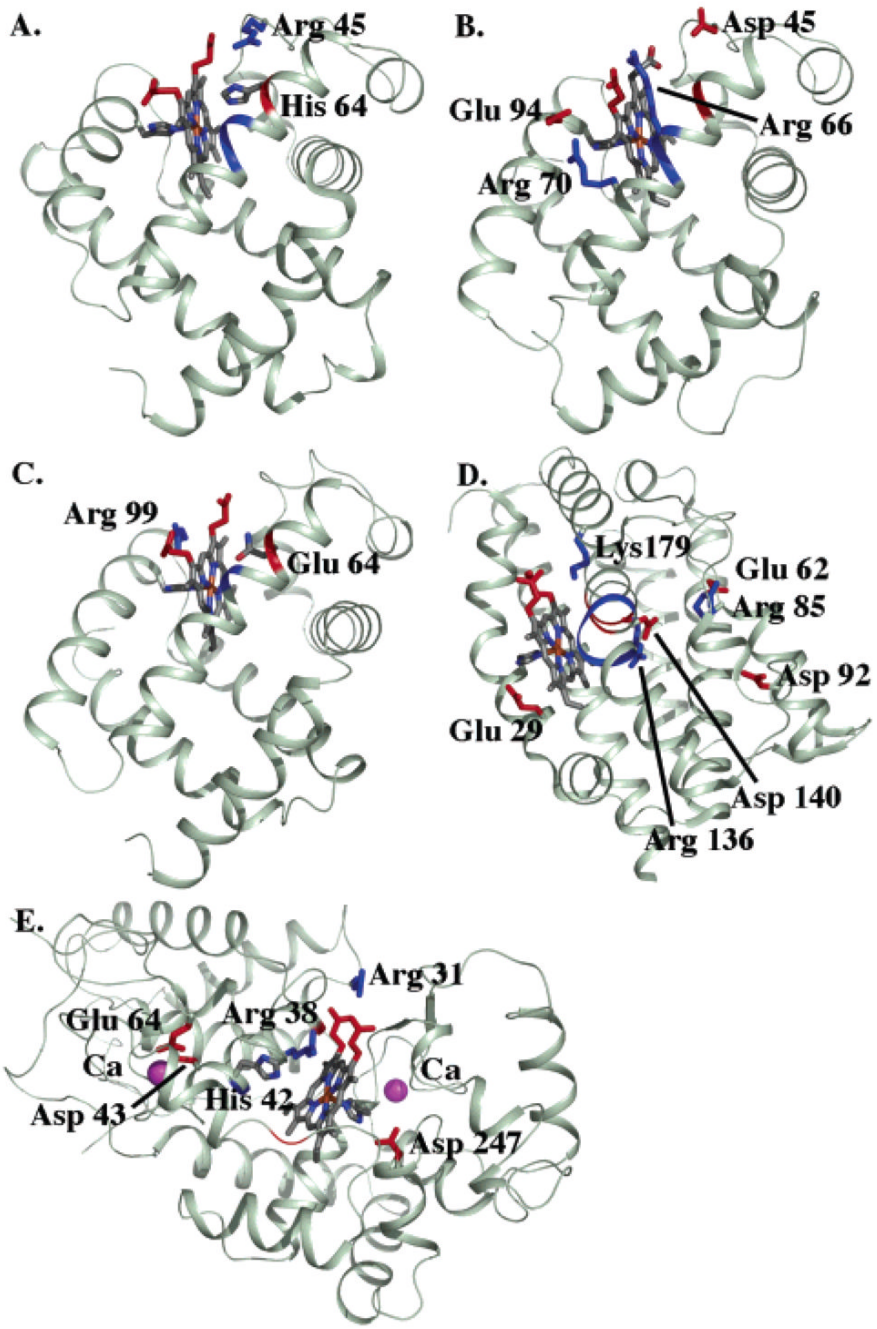

Figure 4.

Structures of (A) sperm whale myoglobin, (B) *Aplysia* myoglobin, (C) hemoglobin I, (D) heme oxygenase, and (E) horseradish peroxidase. Residues and backbone segments that interact with the cationic ferric aquo–heme by more than 0.5 Δp*K* unit (0.68 kcal/mol) are shown.

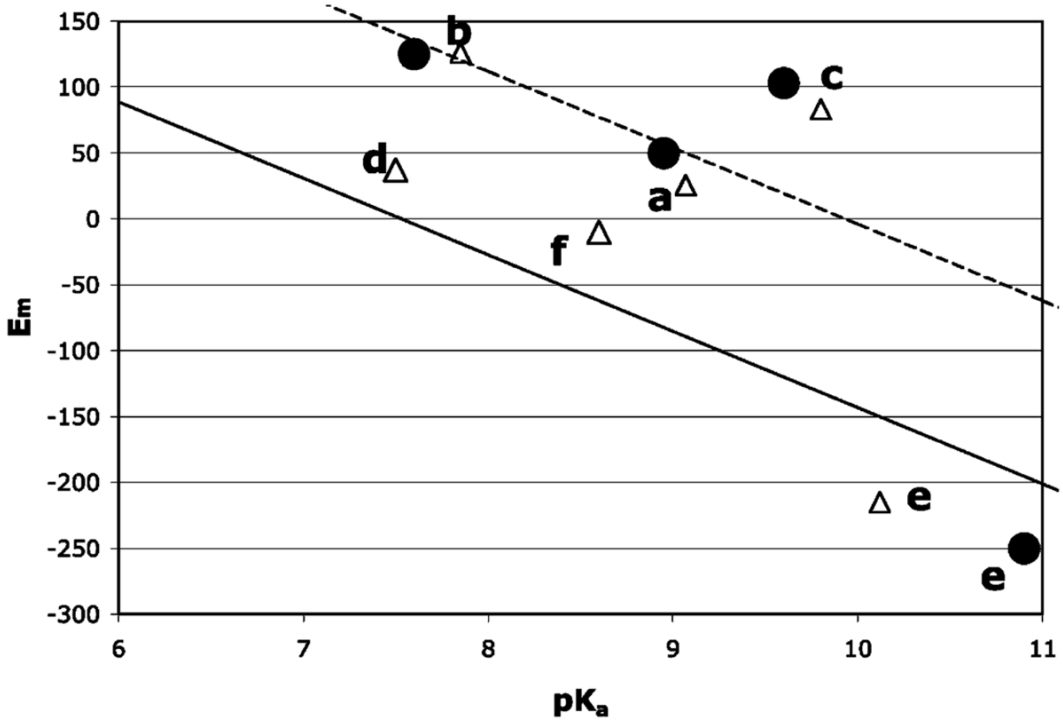

Figure 5.

E_m versus pK_a at pH 7 for (a) sperm whale myoglobin, (b) *Aplysia* myoglobin, (c) hemoglobin I, (d) heme oxygenase, (e) horseradish peroxidase, and (f) cytochrome *c* oxidase. (△) Calculated and (●) available experimental values. The solid line has the same $\Delta\Delta G_{protein}$ for the in situ E_m and pK_a (eqs 2 and 3). The dashed line of $\Delta\Delta G_{protein}$ is 2.4 Δp*K* units larger for E_m than pK_a; 2.4Δp*K* units is the average difference in the $\Delta\Delta G_{rxn}$ for the two types of reactions (Table 1).

Table 1

Experimental and Calculated pK_as and E_ms and Energy Terms Contributing to pK_a and E_m Shifts in the Protein

(a) pK_a of Ferric Aquo–heme

	exp pK_a	**MCCE pK_a**	**$\Delta\Delta G_{rxn}$ (ΔpK unit)**	**ΔG_{pol} (ΔpK unit)**	**ΔG_{res} (ΔpK unit)**
sperm whale myoglobin (7)[a]	8.95 (52)	9.1 ± 1.0	2.07 ± 0.29	0.91 ± 0.14	−2.45 ± 0.83
Aplysia myoglobin (2)	7.6 (52)	7.7 ± 1.0	1.70 ± 0.34	0.88 ± 0.23	−0.75 ± 0.49
hemoglobin I (4)	9.6 (83)	9.8 ± 0.3	1.30 ± 0.18	1.02 ± 0.09	−2.57 ± 0.24
heme oxygenase 1 (5)	7.6 (84,85)	7.5 ± 1.5	0.16 ± 0.37	3.34 ± 0.69	−1.44 ± 1.10
horseradish peroxidase (10)	10.9 (52)	10.1 ± 0.7	1.58 ± 0.39	−0.61 ± 0.07	−1.49 ± 0.66
cyt *c* oxidase (1)	9.0 (53)	8.6	3.9	0.4	−3.3

(b) E_m of Aquo–heme at pH 7

	exp E_m (mV)	MCCE E_m (mV)	$\Delta\Delta G_{rxn}$ (ΔpK unit)	ΔG_{pol} (ΔpK unit)	ΔG_{res} (ΔpK unit)
sperm whale myoglobin (7)	50 (86)	25 ± 33	4.50 ± 0.56	0.98 ± 0.15	−2.97 ± 0.66
Aplysia myoglobin (2)	125 (86)	126 ± 64	4.25 ± 1.24	0.89 ± 0.11	−0.89 ± 0.24
hemoglobin I (4)	103 (87)	83 ± 15	4.33 ± 0.17	0.85 ± 0.12	−1.68 ± 0.09
heme oxygenase 1 (5)	NA	37 ± 13	2.47 ± 0.36	1.84 ± 0.44	−1.61 ± 0.30
horseradish peroxidase (10)	−250 (88,89)	−215 ± 27	3.80 ± 0.51	−0.62 ± 0.06	−4.79 ± 0.49
cyt *c* oxidase[b] (1)	NA	9	5.77	0.77	−5.70

[a] The value in parentheses is the number of PDB files analyzed. NA, not available. Negative free energy terms favor the cationic ferric water–heme raising the aquo–heme pK_a and favor the oxidized heme lowering the E_m. The ferric aquo–heme p$K_{a,sol}$ is 9.6 (70,71). The *b*-type water–hemes have an $E_{m,sol}$ of −120 mV, while the *a*-type heme in cytochrome *c* oxidase has an $E_{m,sol}$ of −20 mV. Hydroxyl–hemes have $E_{m,sol}$s 80 mV lower than the water–hemes (72,73), consistent with the 1.3 pK_a unit shift between the pK_as of ferric and ferrous aquo–heme (70,71).

[b] The pK_a and E_m of the aquo–heme a_3 is calculated with Cu_A oxidized and heme *a* and Cu_B reduced to mimic the experimental pK_a measurements in the CO photolyzed mixed-valence complex (53). 1 ΔpK unit) 58 meV) 1.36 kcal/mol. A systematic shift of −0.74 ΔpK unit (−1 kcal/mol) is added to the reference reaction field energy ($\Delta\Delta G_{RXN,sol}$) of ferric hydroxyl–heme and 0.5 ΔpK unit (0.67 kcal/mol) to ferrous water–heme in deriving the in situ E_ms and pK_as using eqs 2–4.